



Cite this: *Phys. Chem. Chem. Phys.*,
2020, 22, 15381

Gas phase formation of phenalene *via* 10π -aromatic, resonantly stabilized free radical intermediates†

Long Zhao,^a Ralf I. Kaiser,^a Wenchao Lu,^b Musahid Ahmed,^b Artem D. Oleinikov,^{cd} Valeriy N. Azyazov,^{cd} Alexander M. Mebel,^{de} A. Hasan Howlader^e and Stanislaw F. Wnuk^e

For the last few decades, the Hydrogen-Abstraction/aCetylene-Addition (HACA) mechanism has been fundamental in aiding our understanding of the source of polycyclic aromatic hydrocarbons (PAHs) in combustion processes and in circumstellar envelopes of carbon rich stars. However, the reaction mechanisms driving high temperature molecular mass growth beyond triphenylene ($C_{18}H_{12}$) along with the link between PAHs and graphene-type nanostructures as identified in carbonaceous meteorites such as in Murchison and Allende has remained elusive. By exploring the reaction of the 1-naphthyl radical ($C_{10}H_7^*$) with methylacetylene (CH_3CCH) and allene (H_2CCCH_2) under conditions prevalent in carbon-rich circumstellar environments and combustion systems, we provide compelling evidence on a facile formation of 1*H*-phenalene ($C_{13}H_{10}$) – the central molecular building block of graphene-type nanostructures. Beyond PAHs, molecular mass growth processes from 1*H*-phenalene *via* ring-annulation through C3 molecular building blocks may ultimately lead to two-dimensional structures such as graphene nano flakes and after condensation of multiple layers to graphitized carbon. These fundamental reaction mechanisms are of crucial significance to facilitate an understanding of the origin and chemical evolution of carbon in our Galaxy.

Received 25th April 2020,
Accepted 20th June 2020

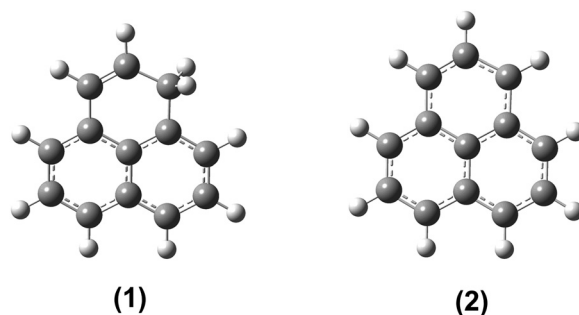
DOI: 10.1039/d0cp02216k

rsc.li/pccp

1. Introduction

Since the groundbreaking isolation of 1*H*-phenalene ($C_{13}H_{10}$) (1) 75 years ago by Lock and Gergely,¹ 1*H*-phenalene (1) together with the phenalenyl radical ($C_{13}H_9^*$) (2)^{2,3} have attracted extensive interest from the (physical)organic,⁴ theoretical,² combustion,⁵ and astrochemical communities. This stems from their electronic structure and chemical bonding acting as prototypes of non-benzoid polycyclic aromatic hydrocarbons (PAHs) and resonantly stabilized free radicals (RSFRs), respectively (Schemes 1 and 2).⁶ The planar 1*H*-phenalene molecule (1) is best characterized as a cyclohexene ring *ortho*- and *peri*-fused to naphthalene and

belongs to the C_s point group with a $^1A'$ electronic ground state. 1*H*-Phenalene possesses a very weak carbon-hydrogen bond at the CH_2 moiety of only 260 kJ mol^{-1} ,⁷ one of the weakest existing C–H bonds on record, compared to a bond energy of 415 kJ mol^{-1} in methane (CH_4).⁸ Hence one of the methylene hydrogen atoms can be easily abstracted or eliminated *via* unimolecular decomposition of 1*H*-phenalene (1) yielding the highly symmetric D_{3h} resonantly stabilized phenalenyl radical (2) holding a $^2A_1''$ electronic ground state. That is to say the presence of an sp^3 hybridized



Scheme 1 Molecular structures of the 1*H*-phenalene molecule (1) and the phenalenyl radical (2).

^a Department of Chemistry, University of Hawaii at Manoa, Honolulu, Hawaii, 96822, USA. E-mail: ralfk@hawaii.edu

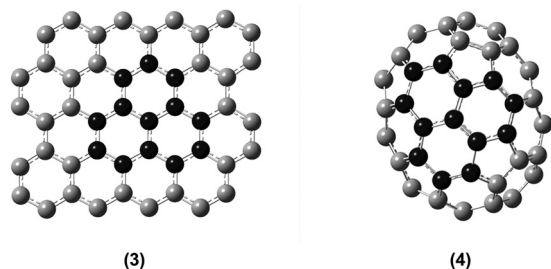
^b Chemical Sciences Division, Lawrence Berkeley National Laboratory, Berkeley, CA 94720, USA. E-mail: mahmed@lbl.gov

^c Department of Physics, Samara National Research University, Samara 443086, Russian Federation. E-mail: mebel@fnu.edu

^d Lebedev Physical Institute, Samara 443011, Russian Federation

^e Department of Chemistry and Biochemistry, Florida International University, Miami, FL 33199, USA

† Electronic supplementary information (ESI) available. See DOI: 10.1039/d0cp02216k



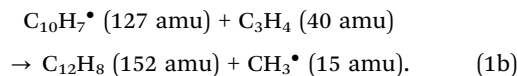
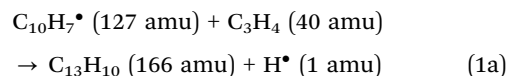
Scheme 2 Molecular building blocks of the *1H*-phenalene carbon skeleton (black) in graphene (3)⁵¹ and C₇₀-fullerene (4).^{52–54}

saturated carbon in *1H*-phenalene (1) prevents the molecule from exhibiting a complete π delocalization over the carbon periphery, with the loss of a hydrogen atom resulting in an energetically favored, delocalized π -system in (2) with phenalenyl (2) affected by Jahn–Teller distortion in its lowest excited $^2E''$ state.^{9,10} Due to this extremely high stabilization, the C–H bond at the CH₂ moiety of *1H*-phenalene is much weaker than the analogous bond at the CH₂ group in indene (327 kJ mol⁻¹)¹¹ and the benzylic bond in the methyl group of toluene (373 kJ mol⁻¹).¹²

The high stability and amphoteric redox nature of this odd-alternant radical (2), which can be oxidized or reduced to a 12 π -electron cation C₁₃H₉⁺ and 14 π -electron anion C₁₃H₉⁻,¹³ prompted the synthesis of exotic organometallic species involving, for instance, iron, chromium, and manganese, in which the phenalenyl moiety bonds in *via* η^1 -, an η^3 -allylic mode, or *via* η^6 -bonding.^{14–21} Competing σ -to- σ and π -to- π dimerization can be modulated by directing the bonding and molecular overlap through functionalization involving bulky side groups such as phenyl (C₆H₅[•]) and tertiary butyl (C(CH₃)₃[•]) with sterically hindering substituents favoring σ -bonding;^{2,3,22–26} the formation of stacked π -dimers of phenalenyl is promoted by removing one electron from the singly occupied molecular orbital (SOMO) of one phenalenyl reactant.² The inherent σ -radical character of the resonance structure of the phenalenyl radical (2) has been recognized as a critical prerequisite of the phenalenyl radical (2) self-association in combustion flames and in deep space potentially leading to benzenoid aromatic structures such as peropyrene (C₂₆H₁₄).²⁷ The identification of the *1H*-phenalene (1) moiety and the phenalenyl radical (2)^{28,29} in pyrolyzed hydrocarbon samples^{5,28,30–32} suggests that phenalenyl (2) and its higher homologues play a critical role in the formation of complex, benzenoid PAHs through reactions with C₂–C₄ alkenes and recombination of phenalenyl (2) with arylmethyl radicals such as naphthylmethyl (C₁₁H₉[•]) or phenanthrenylmethyl (C₁₄H₁₁[•]). Phenalenyl-type radicals were also speculated to play a fundamental role in soot nucleation processes – a kinetic bottleneck in the formation of carbonaceous nanostructures (soot, grains).³³ However, the underlying synthetic routes to *1H*-phenalene (1) itself have remained largely elusive to date with only one pathway to *1H*-phenalene (1), *via* the recombination of the 1-acenaphthyl and methyl radicals, being explored theoretically.⁷

In this study, we untangle synthetic routes to *1H*-phenalene (1) *via* a gas phase synthesis under simulated combustion conditions

involving low-barrier reactions through directed ring expansion reactions involving 10 π aromatic and resonantly stabilized free radical intermediates. Exploiting *1H*-phenalene (1) as a benchmark, we expose the hitherto unknown gas phase chemistry synthesizing *1H*-phenalene (1) (C₁₃H₁₀; 166 amu) – together with its 1-methylacenaphthylene and 3*H*-cyclopenta(a)naphthalene isomers – plus atomic hydrogen (1 amu) *via* the elementary reaction of the 1-naphthyl radical (C₁₀H₇[•]; 127 amu) with allene and methylacetylene (C₃H₄; 40 amu) (reaction (1a)). Our combined experimental and *ab initio* study discloses archetypes of low-barrier reaction pathways guiding the facile formation of *1H*-phenalene (1) *via* molecular mass growth in a reaction of 1-naphthyl with a single allene or methylacetylene molecule. Briefly, *1H*-phenalene (1) was synthesized in a high temperature chemical reactor through a directed synthesis *via* the reaction of the 1-naphthyl radical (C₁₀H₇[•]) with allene (H₂CCCH₂) and methylacetylene (CH₃CCH) at 1350 K and 300 Torr.^{34–36} The products were probed isomer-selectively by exploiting fragment-free photoionization of the products utilizing tunable vacuum ultraviolet (VUV) light in tandem with the detection of the ionized molecules by a high resolution reflectron time-of-flight mass spectrometer (Re-TOF-MS) with mass spectra being collected at intervals of 0.05 eV between 7.30 and 10.00 eV (ESI[†]).



2. Methods

2.1. Experimental method

By studying the reactions of the 1-naphthyl radical (C₁₀H₇[•]) with methylacetylene (CH₃CCH; Organic Technologies; 99%) and allene (H₂CCCH₂; Organic Technologies; 98%) under simulated combustion conditions, we deliver experimental and computational evidence of the molecular growth processes to *1H*-phenalene along with its isomers. Briefly, a continuous beam of 1-naphthyl radicals (C₁₀H₇[•]) was prepared *in situ* through pyrolysis of the 1-iodonaphthalene (C₁₀H₇I) precursor (TCI America, >97%). In three separate experiments, the precursor was kept in a bubbler at room temperature and seeded in pure helium (blank experiment) and in the hydrocarbon gases (methylacetylene and allene) at pressures of 300 Torr. Each gas mixture was then expanded into a resistively heated silicon carbide (SiC) tube (“pyrolytic reactor”) held at 1350 ± 10 K as monitored by a Type-C thermocouple. The hydrocarbon gases serve not only as seeding gases, but also as reactants with the pyrolytically generated 1-naphthyl radicals. The products formed in the reactor were expanded supersonically, passed through a 2 mm diameter skimmer located 10 mm downstream of the pyrolytic reactor, and entered into the photoionization chamber, which houses the Wiley–McLaren reflectron time-of-flight mass spectrometer (Re-TOF-MS).

The quasi-continuous tunable synchrotron VUV light from the Advanced Light Source (ALS) intercepted the neutral molecular beam perpendicularly in the extraction region of the Re-TOF-MS. VUV single photon ionization is essentially a fragment-free ionization technique and is compared soft to electron impact ionization.³⁷ The ions formed *via* photoionization are extracted and detected by a multichannel plate (MCP) detector. Photoionization efficiency (PIE) curves, which report ion counts as a function of photon energy with a step interval of 0.05 eV at a well-defined mass-to-charge ratio (*m/z*), were produced by integrating the signal recorded at the specific *m/z* for the species of interest from 7.30 eV to 10.00 eV. It shall be noted that under these experimental conditions, methylacetylene and allene do not isomerize to each other in the pyrolysis tube.^{38,39} Detailed computational fluid dynamics (CFD) simulations of the gas flow in the microreactor suggest residence times of the reactants of a few 100 μ s.^{36,40,41} Typically, at the reaction center, this would give rise to a few tens collisions between the 1-naphthyl radical and the allene/methylacetylene molecules and/or between reaction products. PIE calibration curves for helium-seeded $C_{13}H_{10}$ isomers were also collected (Fig. S1, ESI[†]), to identify the products of interest observed in this work. Synthesis and characterization of 1*H*-phenalene and 1-methylacenaphthylene are described in the ESI.[†]

2.2. Computational methods

Geometries of the reactants and products of the reactions of 1-naphthyl with allene and methylacetylene and various intermediates and transition states on the $C_{13}H_{11}$ potential energy surface (PES) were optimized at the density functional B3LYP/6-311G(d,p) level of theory and their vibrational frequencies were computed using the same theoretical method. Single-point energies were then refined at the G3(MP2,CC) level using a series of coupled clusters CCSD(T) and second-order Møller-Plesset perturbation theory MP2 calculations, where the final energy was computed as

$$E[G3(MP2,CC)] = E[CCSD(T)/6-311G(d,p)] + E[(MP2/G3Large)] - E[MP2/6-311G(d,p)] + ZPE[B3LYP/6-311G(d,p)]^{42-44}$$

The G3(MP2,CC) model chemistry approach normally provides chemical accuracy of 0.01–0.02 Å for bond lengths, 1–2° for bond angles, and 3–6 kJ mol⁻¹ for relative energies of hydrocarbons, their radicals, reaction energies, and barrier heights in terms of average absolute deviations.⁴³ The GAUSSIAN 09⁴⁵ and MOLPRO 2010⁴⁶ program packages were used for the *ab initio* calculations. Pressure- and temperature-dependent rate constants for the 1-naphthyl + C_3H_4 reactions at different temperatures and pressures were evaluated using the Rice–Ramsperger–Kassel–Marcus Master Equation (RRKM-ME) theoretical approach utilizing the MESS software package.^{47,48} Here, densities of states and partition functions for local minima and numbers of states for transition states were computed within the Rigid-Rotor, Harmonic-Oscillator (RRHO) model. For critical entrance transition states of allene/methylacetylene addition to 1-naphthyl, low-frequency normal modes corresponding to internal rotations were treated as one-dimensional hindered rotors in partition function calculations, where the corresponding vibrational

frequencies were removed. Corresponding one-dimensional torsional potentials were calculated by scanning PESs at the B3LYP/6-311G(d,p) level of theory. Tunneling corrections using asymmetric Eckart potentials were included in rate constant calculations. We employed collision parameters used by us earlier for RRKM-ME calculations of the prototype $C_6H_5 + C_3H_4$ ⁴⁹ and 1-naphthyl + C_3H_4 reactions;³⁸ the Lennard-Jones parameters were taken as (ϵ/cm^{-1} , $\sigma/\text{Å}$) = (390, 4.46) and the temperature dependence of the range parameter α for the deactivating wing of the energy transfer function was expressed as $\alpha(T) = \alpha_{300}(T/300 \text{ K})^n$, with $n = 0.62$ and $\alpha_{300} = 424 \text{ cm}^{-1}$. Calculations at $p = 10^{-10}$ atm emulating the zero-pressure limit took into account radiational stabilization of $C_{13}H_{11}$ intermediates. Additional details of RRKM-ME calculations can be found in our previous publications⁴⁹ and in the input file for the MESS package given as Note S1 (ESI[†]).

3. Experimental results

We analyzed first the mass spectra of the 1-naphthyl-allene and 1-naphthyl-methylacetylene systems qualitatively and extract the molecular formulae of the reaction products related to the formation of 1*H*-phenalene (**1**). Illustrative mass spectra recorded at a photoionization energy of 9.50 eV are presented in Fig. 1 for the reactions of 1-naphthyl with allene and methylacetylene (Fig. 1a and b) to reveal the molecular formula of reaction (1a) and (1b). Replacing the hydrocarbon reactant (allene, methylacetylene) with non-reactive helium carrier gas (Fig. 1c) confirmed that the products (Fig. 1a and b) are synthesized as a result of the reaction of the 1-naphthyl radical with allene and methylacetylene, but not from decomposition

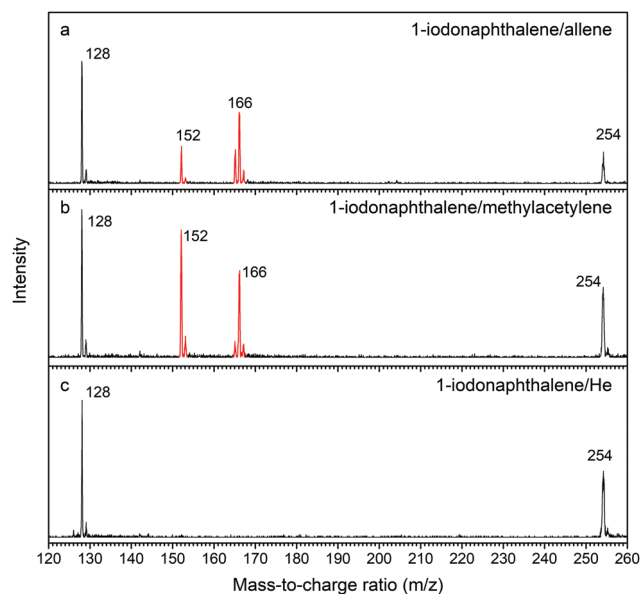


Fig. 1 Comparison of photoionization mass spectra recorded at a photon energy of 9.50 eV. (a) 1-iodonaphthalene ($C_{10}H_7I$)–allene (C_3H_4) system; (b) 1-iodonaphthalene ($C_{10}H_7I$)–methylacetylene (C_3H_4) system; and (c) 1-iodonaphthalene ($C_{10}H_7I$)–helium (He) system. The mass peaks of the newly formed species along with the ^{13}C -counterparts are highlighted in red.

of the 1-naphthyl radicals. An analysis of these mass spectra discloses the formation of molecules with the molecular formulae $C_{13}H_{10}$ (166 amu) and $C_{12}H_8$ (152 amu) along with the ^{13}C isotopologues at $m/z = 167$ and 153 in both systems. Further, signal is observable for $C_{13}H_9$ (165 amu). These ion counts are clearly absent in the control experiments suggesting that molecules detected *via* $m/z = 152, 153, 165, 166,$ and 167 signify reaction products in both $C_{10}H_7-C_3H_4$ systems. Considering the molecular weight of the reactants and the products, the $C_{13}H_{10}$ isomer(s) along with atomic hydrogen are the result of the reaction of the 1-naphthyl radical with allene/methylacetylene *via* channel (1a). Signal at $C_{12}H_8$ (152 amu) can be linked with the methyl (CH_3^*) loss channel in reaction (1b). Reaction channel(s) attributed to $C_{13}H_9$ (165 amu) are revealed below. The ion counts at m/z of 254 ($C_{10}H_7I^+$), 128 ($C_{10}H_8^+$), and 129 ($C_9^{13}CH_8^+$) are detectable in the control experiments as well and hence cannot be linked to the reaction of 1-naphthyl radicals with allene/methylacetylene. These species are associated with the 1-iodonaphthalene precursor (254 amu) and naphthalene ($C_{10}H_8$) with the latter likely formed through recombination of 1-naphthyl with a hydrogen atom.

The investigation of the mass spectra delivered convincing evidence on the formation of $C_{13}H_{10}$ (166 amu) and $C_{12}H_8$ (152 amu) isomer(s) along with their ^{13}C analogous species $C_{12}^{13}CH_{10}$ (167 amu) and $C_{11}^{13}CH_8$ (153 amu) through the reaction of 1-naphthyl with allene and methylacetylene (reactions (1a)/(1b)); also, contributions of $C_{13}H_9$ (165 amu) isomer(s) are likely. The primary interest is, however, to elucidate which isomer(s) is/are formed. This necessitates an in-depth analysis of the underlying photoionization efficiency (PIE) curves of the mass-to-charge ratios of interest (Fig. 2) to reveal

the isomers formed. Each PIE curve reports the ion counts at a well-defined m/z ratio such as $m/z = 166$ as a function of the photon energy from 7.30 eV to 10.00 eV (Fig. 2). The shapes of the PIE curves of $C_{13}H_{10}$ isomers – 1*H*-phenalene, 3*H*-cyclopenta(a)naphthalene, 1-methylacenaphthylene are very different and therefore unique as recorded in separate calibration experiments within the same experimental setup under identical experimental conditions (Fig. S1, ESI†).³⁸ A linear combination of these are used to fit the experimental PIE curves, shown for $m/z = 165, 166,$ and 167 (Fig. 2). Even after scaling, these PIE curves are not superimposable suggesting that $m/z = 165$ does not represent a fragment of $m/z = 166$, but rather distinct isomer(s) of $C_{13}H_9$ (165 amu). Since no reference curves of any $C_{13}H_9$ isomer exists, we conclude that although $C_{13}H_9$ isomer(s) are formed, it is not feasible to elucidate the actual structure(s) at the present stage. However, considering a 1.1% natural abundance of ^{13}C , 14.3% of the ion signal of $m/z = 165$ ($C_{13}H_9^+$) has to contribute to ion counts of $m/z = 166$ ($C_{12}^{13}CH_9^+$) (Fig. 2). Fitting of the PIE curves at $m/z = 166$ ($C_{12}^{13}CH_9^+/C_{13}H_{10}^+$) reveals the formation of three $C_{13}H_{10}$ isomers: 1*H*-phenalene (**p1**), 1-methylacenaphthylene (**p8**), and 3*H*-cyclopenta(a)naphthalene (**p2**) (Fig. 2). Branching ratios of the ion counts of these isomers were derived at 10.0 eV for the 1-naphthyl – allene and 1-naphthyl – methylacetylene system to be $32 \pm 3\%$ (**p1**), $38 \pm 4\%$ (**p8**), and $30 \pm 3\%$ (**p2**) as well as $28 \pm 3\%$ (**p1**), $61 \pm 6\%$ (**p8**), and $11 \pm 1\%$ (**p2**), respectively. 1*H*-Phenalene is more abundant in the 1-naphthyl-allene system at the expense of 1-methylacenaphthylene, which dominates the ion counts in the 1-naphthyl-methylacetylene system. We emphasize that the aforementioned contributions to the fit of the experimental PIE curve do not represent the product

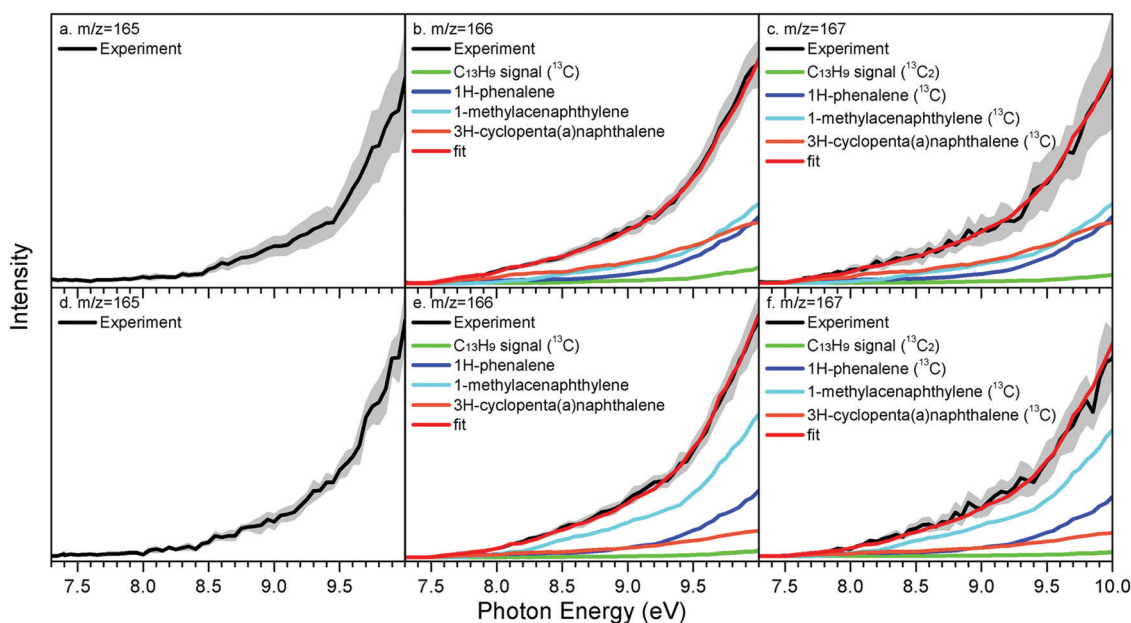


Fig. 2 Photoionization efficiency (PIE) curves for signal at $m/z = 165$ to 167 in the systems of (a)–(c): 1-iodonaphthalene ($C_{10}H_7I$) + allene (C_3H_4); (d)–(f): 1-iodonaphthalene ($C_{10}H_7I$) + methylacetylene (C_3H_4). Black: experimentally derived PIE curves; colored lines (green, blue, cyan and brown): reference PIE curves; red lines: overall fit. The overall error bars consist of two parts: $\pm 10\%$ based on the accuracy of the photodiode and a 1σ error of the PIE curve averaged over the individual scans.

branching ratios since absolute ionization cross sections are not available for any of the $C_{13}H_{10}$ isomers. However, the experiments provide explicit evidence and the proof-of-concept that the reaction of 1-naphthyl with allene and methylacetylene leads to the formation of three distinct $C_{13}H_{10}$ isomers: 1*H*-phenalene (**p1**), 1-methylacenaphthylene (**p8**), and 3*H*-cyclopenta(a)naphthalene (**p2**). The corresponding PIE curves of $m/z = 167$ ($C_{11}^{13}C_2H_9^+/C_{12}^{13}CH_{10}^+$) match these findings and reveal that ion signal at $m/z = 167$ originate predominantly from the aforementioned ^{13}C -isotopologue PAHs ($C_{13}H_{10}$) and to a minor amount from doubly ^{13}C substituted $C_{13}H_9$ radicals.

4. Discussion

The experimental data provide explicit evidence on the detection of 1*H*-phenalene ($C_{13}H_{10}$) (**p1**) along with two of its isomers (1-methylacenaphthylene (**p8**), 3*H*-cyclopenta(a)naphthalene (**p2**)) and acenaphthylene ($C_{12}H_8$) (**p9**) formed *via* the elementary reactions of 1-naphthyl with allene and methylacetylene in the gas phase. Coupling these experimental finding with electronic structure calculations allows us to untangle the synthetic routes (Fig. 3 and Fig. S3, ESI[†]) for these complex processes. Our computations disclose that the 1-naphthyl radical adds to the π -electron density of the terminal (C1) or central carbon atom (C2) of the methylacetylene or allene reactants yielding intermediates **i1** and **i5** or **i8** and **i10**, respectively.

These processes involve small barriers to addition of only 5 to 11 kJ mol^{-1} . These doublet intermediates can isomerize *via* the low energy reaction sequence **i1** \rightarrow **i2** \rightarrow **i3** \rightarrow **i4** \rightarrow **i5** \rightarrow **i7** \rightarrow **i8** involving *cis-trans* isomerization, a shift of the naphthyl group from the terminal to the central carbon in the side chain *via* three-member ring cyclization followed by the three-member ring opening, and consecutive hydrogen shifts from the naphthyl moiety to the side chain (**i5** \rightarrow **i7**) and *vice versa* (**i7** \rightarrow **i8**). Further, the **i8** intermediate is connected to the complex **i10** of the 1-naphthyl – allene system *via* a similar shift of the naphthyl group from the central to the terminal carbon atom of allene occurring *via* intermediate **i9** featuring a three-member ring. It is important to highlight that both the 1-naphthyl – methylacetylene and 1-naphthyl – allene surfaces are connected *via* intermediate **i8**. The doublet radical intermediate **i8** is central to rationalize that in both systems, the same reaction channels leading to 1*H*-phenalene ($C_{13}H_{10}$) (**p1**, *via* **i8**, **i9**, **i10**, **i13**, and **i14**) and 3*H*-cyclopenta(a)naphthalene ($C_{13}H_{10}$) (**p2**, *via* **i8**, **i9**, **i10**, **i11**, and **i12**) are open, whereas 1-methylacenaphthylene ($C_{13}H_{10}$) (**p8**), and acenaphthylene ($C_{12}H_8$) (**p9**) are produced *via* the intermediates **i2**, **i21**, and **i22**. Here, **i2** can be formed in one step in the 1-naphthyl – methylacetylene system or *via* the reaction sequence **i8** \rightarrow **i7** \rightarrow **i5** \rightarrow **i4** \rightarrow **i3** \rightarrow **i2** in the 1-naphthyl – allene system. Interestingly, **i8** together with the less important **i15** and **i16** intermediates represent resonantly stabilized allylic radicals also containing a 10π aromatic naphthalene moiety. Due to this resonance stabilization, **i8**,

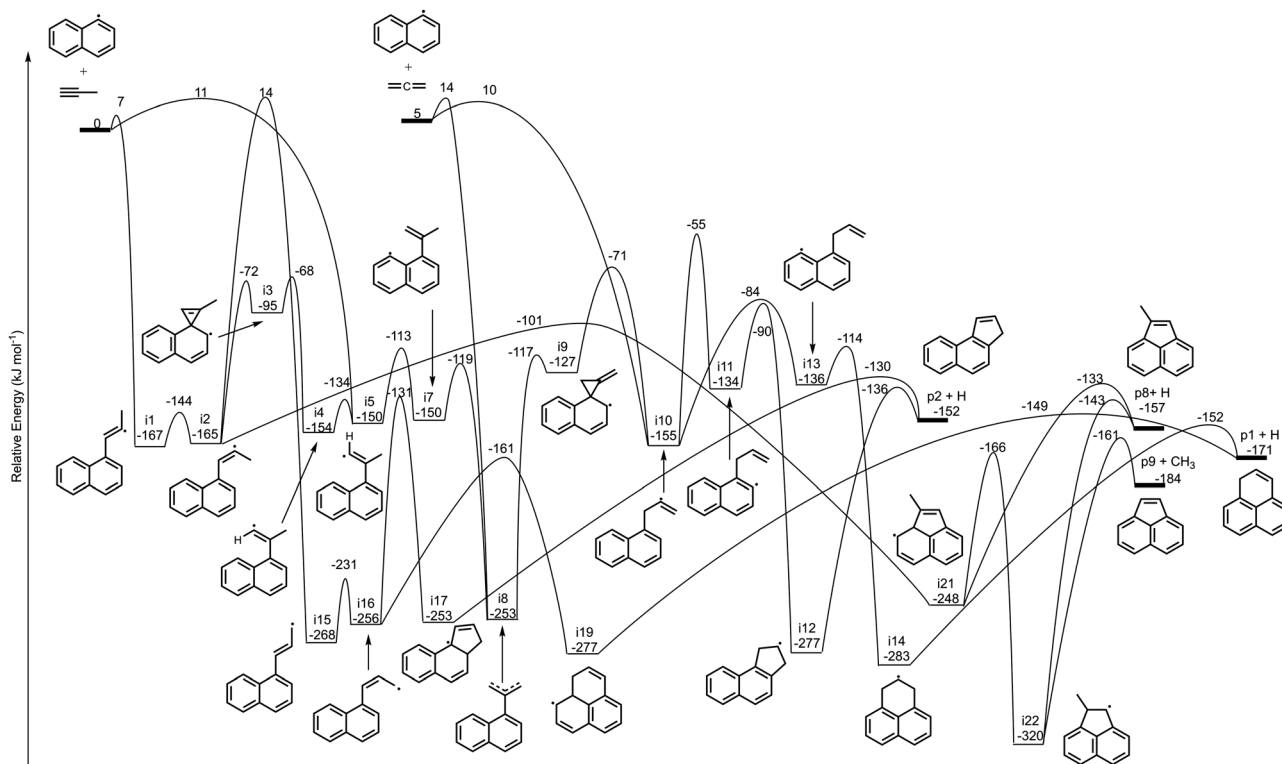


Fig. 3 Potential energy surface (PES) for the 1-naphthyl ($C_{10}H_7^*$) reaction with allene/methylacetylene (C_3H_4). This PES was calculated at the G3(MP2,CC)//B3LYP/6-311G(d,p) level of theory for the channels leading to 1*H*-phenalene (**p1**), 3*H*-cyclopenta(a)naphthalene (**p2**), 1-methylacenaphthylene (**p8**), and acenaphthylene (**p9**). The relative energies are given in kJ mol^{-1} . The complete PES is provided in the ESI[†].

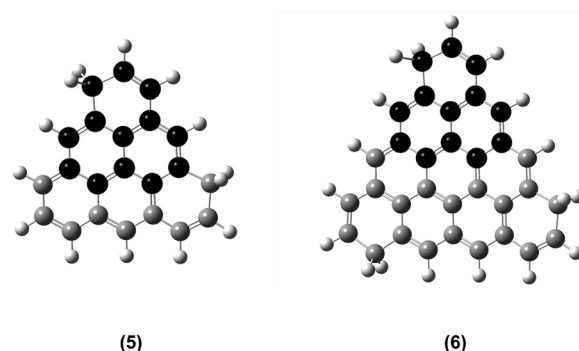
i15, and **i16** reside 100 or more kJ mol^{-1} lower in energy than similar two-ring-side-chain intermediates **i1**, **i2**, **i4**, **i5**, **i7**, **i10**, **i11**, and **i13**. The calculated potential energy diagram also suggests that isomerization of **i2** to **i15**, **i16**, and then **i19** or **i17**, followed by formation of 1*H*-phenalene(**p1**) or 3*H*-cyclopenta(a)naphthalene (**p2**) along with atomic hydrogen are unfavorable due to inherent barrier height of 179 kJ mol^{-1} involved in the hydrogen migration **i2** \rightarrow **i15** compared to the more facile cyclization of **i2** to **i3** and five-member ring closure **i2** \rightarrow **i21**. The existence of intermediate **i10** is central to understand the underlying reaction mechanism(s). The facile reaction sequence *via* **i13** and **i14** through ring expansion leads *via* hydrogen elimination to 1*H*-phenalene ($\text{C}_{13}\text{H}_{10}$) (**p1**); likewise, intermediate **i10** can undergo unimolecular decomposition to form 3*H*-cyclopenta(a)naphthalene (**p2**) and 1*H*-cyclopenta(a)naphthalene (**p3**).

The latter two products are predicted by our RRKM-Master Equation calculations to have very similar branching ratios of 4% as compared to $\sim 40\%$ for **p1** at the experimental temperature of $1350 \pm 10 \text{ K}$ (see Table S1; the computed **p1** branching ratios are 42.2% at 1300 K and 37.6% at 1400 K, ESI[†]). Since the reaction pathways leading to **p1** and **p2/p3** both proceed *via* the common intermediate **i10** (Fig. 3 and Fig. S3, ESI[†]), the larger yield of **p1** as compared to **p2** and **p3** can be attributed to the higher barrier for isomerization of **i10** to **i11** (1,4-hydrogen shift) compared to **i13** (1,5-hydrogen shift), where the production of **i11** is unavoidable to form **i12**, which then fragments to **p2** or **p3** (Fig. S3, ESI[†]), whereas **p1** is produced *via* **i13** and **i14**. The failed detection of **p3** might be explained by its small photoionization cross section; interestingly, 1*H*-cyclopenta(a)-naphthalene (**p3**) could not be detected in our earlier study of the 2-naphthyl – allene/methylacetylene systems, where its computed branching ratio is also similar to that of 3*H*-cyclopenta(a)naphthalene (**p2**).³⁸ As noted above, the alternative channel to form **p2** *via* **i17** is hindered by the high barrier for the **i2** \rightarrow **i15** step. Besides **i10**, which is central to rationalize the formation of **p1** and **p2**, intermediate **i2** is of fundamental importance to understand the detection of acenaphthylene (C_{12}H_8) (**p9**) and 1-methylacenaphthylene ($\text{C}_{13}\text{H}_{10}$) (**p8**). Intermediate **i2** can undergo a facile five-member ring closure to **i21** which then either ejects a hydrogen atom to form 1-methylacenaphthylene ($\text{C}_{13}\text{H}_{10}$) (**p8**) or isomerizes to **i22** prior to emission of a methyl group along with formation of acenaphthylene (C_{12}H_8) (**p9**). The overall reactions are exoergic and all transition states involved for the isomerization processes lie below the energy of the separated reactants. 1-Ethynyl-naphthalene (C_{12}H_8) (**p7**) can be produced by the CH_3 group loss from **i4**. No substituted naphthalene species (**p4–p6**) which can be formed *via* 1-naphthyl addition – hydrogen atom elimination (Fig. S3, ESI[†]) were detected. This finding is supported by statistical calculations revealing that the thermodynamically more favorable 1*H*-phenalene ($\text{C}_{13}\text{H}_{10}$) (**p1**) formation along with the tricyclic aromatic systems **p2**, **p8**, and **p9** is preferred, and that under our experimental conditions, multi-step reaction sequences *via* addition – hydrogen shifts – cyclization – hydrogen/methyl elimination are favorable compared to ‘simple’ addition – hydrogen

elimination steps (Table S1, ESI[†]). It should be noted however that the statistical calculations predict a rapid growth of the entropically favorable products **p4** and **p7** (methylacetylene) and **p5** and **p6** (allene) with the temperature increase beyond 1500 K. Under real combustion conditions, **p4–p6** can be converted to the thermodynamically preferable phenalene, cyclopenta(a)naphthalenes, and 1-methylacenaphthylene *via* hydrogen-assisted isomerization. At very low pressures, the formation of 1*H*-phenalene (**p1**) is clearly preferable for the 1-naphthyl – allene system up to 1500 K (Fig. S5 and Table S1, ESI[†]), whereas the 1-naphthyl – methylacetylene system is dominated by the production of **p9** plus methyl and **p8** plus atomic hydrogen also up to 1500 K (Fig. S5 and Table S2, ESI[†]).

5. Conclusion

To conclude, our joint experimental and computational investigation delivers explicit proof on the formation of 1*H*-phenalene through molecular mass growth processes in a reaction of 1-naphthyl with allene and methylacetylene in the gas phase. Rather than traditional bay closures in aromatic radicals involving the hydrogen abstraction – acetylene addition (HACA) mechanism such as the formation of phenanthrene ($\text{C}_{14}\text{H}_{10}$) and pyrene ($\text{C}_{16}\text{H}_{10}$) *via* the reactions of biphenyl ($\text{C}_{12}\text{H}_9^\bullet$)⁵⁰ and 4-phenanthryl ($\text{C}_{14}\text{H}_9^\bullet$)³⁵ with the C2 building block acetylene (C_2H_2) [C4–C2 annulation], the present study reveals a hitherto unfamiliar bay closure pathway through ring annulation involving an aromatic radical (1-naphthyl) plus a C3 hydrocarbon (methylacetylene, allene) [C3–C3 annulation]. This mechanism might be fundamental in aiding our understanding of molecular mass growth processes of graphene nano flakes and graphene sheets starting from 1*H*-phenalene *via* peripheral expansion of the 1*H*-phenalene moiety to triangular graphene-type molecules 1,5-dihydrodibenzo[*cd,mn*]pyrene ($\text{C}_{22}\text{H}_{14}$) and 6,11-dihydro-1*H*-tribenzo[*bc,hi,no*] coronene ($\text{C}_{33}\text{H}_{18}$) (Scheme 3).⁶ This pathway could also explain the detection of graphitized carbon with grain sizes of up to 80 nm as probed in carbonaceous chondrites like Allende and Murchison, which are likely formed *via* condensation of multiple layers to



Scheme 3 Molecular mass growth processes involving the 1*H*-phenalene molecule (**1**) *via* peripheral expansion of the 1*H*-phenalene moiety to triangular graphene-type molecules 1,5-dihydrodibenzo[*cd,mn*]pyrene (**5**) and 6,11-dihydro-1*H*-tribenzo[*bc,hi,no*]coronene (**6**).

graphene-like nanostructures.³⁵ In circumstellar envelopes of carbon-rich stars with temperatures of up to a few 1000 K and even in combustion flames, the entrance barriers to addition can be overcome easily thus providing a versatile, hitherto overlooked pathways to two dimensional nanostructures in oxygen poor combustion systems and in deep space with aryl radicals and methylacetylene and allene centered molecular building blocks.

Conflicts of interest

There are no conflicts to declare.

Acknowledgements

This work was supported by the US Department of Energy, Basic Energy Sciences DE-FG02-03ER15411 and DE-FG02-04ER15570 to the University of Hawaii (RIK) and Florida International University (AMM), respectively. M. A. is supported by the Director, Office of Science, Office of Basic Energy Sciences, of the U.S. Department of Energy under Contract No. DE-AC02-05CH11231, through the Gas Phase Chemical Physics program of the Chemical Sciences Division. The ALS is supported under the same contract. *Ab initio* and RRKM-ME calculations at Samara University were supported by the Ministry of Higher Education and Science of the Russian Federation under Grant No. 14.Y26.31.0020.

References

- G. Lock and G. Gergely, *Ber. Dtsch. Chem. Ges.*, 1944, **77**, 461–465.
- D. Small, V. Zaitsev, Y. Jung, S. V. Rosokha, M. Head-Gordon and J. K. Kochi, *J. Am. Chem. Soc.*, 2004, **126**, 13850–13858.
- Z. Mou, K. Uchida, T. Kubo and M. Kertesz, *J. Am. Chem. Soc.*, 2014, **136**, 18009–18022.
- R. C. Haddon, *Aust. J. Chem.*, 1975, **28**, 2343–2351.
- S. V. Kalpathy, N. B. Poddar, S. P. Bagley and M. J. Wornat, *Proc. Combust. Inst.*, 2015, **35**, 1833–1841.
- A. M. Toader, C. M. Buta, B. Frecus, A. Mischie and F. Cimpoesu, *J. Phys. Chem. C*, 2019, **123**, 6869–6880.
- D. P. Porfiriev, V. N. Azyazov and A. M. Mebel, *Combust. Flame*, 2020, **213**, 302–313.
- Y.-R. Luo, *Comprehensive Handbook of Chemical Bond Energies*, Boca Raton, CRC Press, 2007.
- W. Cofino, S. van Dam, D. Kamminga, G. P. Hoornweg, C. Gooijer, C. MacLean and N. Velthorst, *Mol. Phys.*, 1984, **51**, 537–550.
- G. D. O'Connor, T. P. Troy, D. A. Roberts, N. Chalyavi, B. Fückel, M. J. Crossley, K. Nauta, J. F. Stanton and T. W. Schmidt, *J. Am. Chem. Soc.*, 2011, **133**, 14554–14557.
- L. Zhao, M. B. Prendergast, R. I. Kaiser, B. Xu, W. Lu, U. Ablikim, M. Ahmed, A. D. Oleinikov, V. N. Azyazov, A. M. Mebel, A. H. Howlader and S. F. Wnuk, *ChemPhysChem*, 2019, **20**, 1437–1447.
- C. L. Rasmussen, M. S. Skjøth-Rasmussen, A. D. Jensen and P. Glarborg, *Proceedings of the Combustion Institute*, 2005, **30**, 1023–1031.
- C. Puzzarini, A. Baiardi, J. Bloino, V. Barone, T. E. Murphy, D. H. Drew and A. Ali, *Astron. J.*, 2017, **154**, 82.
- X. Chi, M. E. Itkis, K. Kirschbaum, A. A. Pinkerton, R. T. Oakley, A. W. Cordes and R. C. Haddon, *J. Am. Chem. Soc.*, 2001, **123**, 4041–4048.
- X. Chi, M. Itkis, B. Patrick, T. Barclay, R. Reed, R. Oakley, A. Cordes and R. Haddon, *J. Am. Chem. Soc.*, 1999, **121**, 10395–10402.
- P. A. Koutentis, Y. Chen, Y. Cao, T. P. Best, M. E. Itkis, L. Beer, R. T. Oakley, A. W. Cordes, C. P. Brock and R. C. Haddon, *J. Am. Chem. Soc.*, 2001, **123**, 3864–3871.
- S. K. Pal, M. E. Itkis, R. W. Reed, R. T. Oakley, A. W. Cordes, F. S. Tham, T. Siegrist and R. C. Haddon, *J. Am. Chem. Soc.*, 2004, **126**, 1478–1484.
- M. Itkis, X. Chi, A. Cordes and R. Haddon, *Science*, 2002, **296**, 1443–1445.
- J. S. Müller, *Angew. Chem., Int. Ed.*, 2003, **42**, 27–29.
- Ž. Tomović, M. D. Watson and K. Müllen, *Angew. Chem., Int. Ed.*, 2004, **43**, 755–758.
- D. Griller and K. U. Ingold, *Acc. Chem. Res.*, 1976, **9**, 13–19.
- V. Zaitsev, S. V. Rosokha, M. Head-Gordon and J. K. Kochi, *J. Org. Chem.*, 2006, **71**, 520–526.
- D. Small, S. V. Rosokha, J. K. Kochi and M. Head-Gordon, *J. Phys. Chem. A*, 2005, **109**, 11261–11267.
- B. Kolb, M. Kertesz and T. Thonhauser, *J. Phys. Chem. A*, 2013, **117**, 3642–3649.
- F. Mota, J. S. Miller and J. J. Novoa, *J. Am. Chem. Soc.*, 2009, **131**, 7699–7707.
- S. Suzuki, Y. Morita, K. Fukui, K. Sato, D. Shiomi, T. Takui and K. Nakasuji, *J. Am. Chem. Soc.*, 2006, **128**, 2530–2531.
- K. Uchida, S. Ito, M. Nakano, M. Abe and T. Kubo, *J. Am. Chem. Soc.*, 2016, **138**, 2399–2410.
- J. E. Bennett, *Proc. Chem. Soc., London*, 1961, 144–145.
- N. Senglet, D. Faure, T. Des Courieres, C. Bernasconi and R. Guillard, *Fuel*, 1990, **69**, 203–206.
- E. A. Hurst, N. B. Poddar, K. Vutukuru, S. V. Kalpathy and M. J. Wornat, *Proc. Combust. Inst.*, 2019, **37**, 1107–1115.
- S. S. Kim, M. L. Jarand and K. Durai-Swamy, *Fuel*, 1982, **61**, 1124–1126.
- F. Gerson, *Helv. Chim. Acta*, 1966, **49**, 1463–1467.
- K. O. Johansson, M. P. Head-Gordon, P. E. Schrader, K. R. Wilson and H. A. Michelsen, *Science*, 2018, **361**, 997–1000.
- L. Zhao, R. I. Kaiser, B. Xu, U. Ablikim, M. Ahmed, M. M. Evseev, E. K. Bashkurov, V. N. Azyazov and A. M. Mebel, *Nat. Astron.*, 2018, **2**, 973–979.
- L. Zhao, R. I. Kaiser, B. Xu, U. Ablikim, M. Ahmed, D. Joshi, G. Veber, F. R. Fischer and A. M. Mebel, *Nat. Astron.*, 2018, **2**, 413–419.
- L. Zhao, R. I. Kaiser, B. Xu, U. Ablikim, M. Ahmed, M. V. Zagidullin, V. N. Azyazov, A. H. Howlader, S. F. Wnuk and A. M. Mebel, *J. Phys. Chem. Lett.*, 2018, **9**, 2620–2626.
- F. Qi, *Proc. Combust. Inst.*, 2013, **34**, 33–63.

- 38 L. Zhao, M. Prendergast, R. I. Kaiser, B. Xu, U. Ablikim, W. Lu, M. Ahmed, A. D. Oleinikov, V. N. Azyazov and A. H. Howlader, *Phys. Chem. Chem. Phys.*, 2019, **21**, 16737–16750.
- 39 F. Zhang, R. I. Kaiser, V. V. Kislov, A. M. Mebel, A. Golan and M. Ahmed, *J. Phys. Chem. Lett.*, 2011, **2**, 1731–1735.
- 40 L. Zhao, R. I. Kaiser, B. Xu, U. Ablikim, W. Lu, M. Ahmed, M. M. Evseev, E. K. Bashkirov, V. N. Azyazov, M. V. Zagidullin, A. N. Morozov, A. H. Howlader, S. F. Wnuk, A. M. Mebel, D. Joshi, G. Veber and F. R. Fischer, *Nat. Commun.*, 2019, **10**, 1510.
- 41 M. Zagidullin, R. Kaiser, D. Porfiriev, I. Zavershinskiy, M. Ahmed, V. Azyazov and A. Mebel, *J. Phys. Chem. A*, 2018, **122**, 8819–8827.
- 42 L. A. Curtiss, K. Raghavachari, P. C. Redfern, V. Rassolov and J. A. Pople, *J. Chem. Phys.*, 1998, **109**, 7764–7776.
- 43 L. A. Curtiss, K. Raghavachari, P. C. Redfern, A. G. Baboul and J. A. Pople, *Chem. Phys. Lett.*, 1999, **314**, 101–107.
- 44 A. G. Baboul, L. A. Curtiss, P. C. Redfern and K. Raghavachari, *J. Chem. Phys.*, 1999, **110**, 7650–7657.
- 45 M. J. Frisch, G. W. Trucks, H. B. Schlegel, G. E. Scuseria, M. A. Robb, J. R. Cheeseman, G. Scalmani, V. Barone, B. Mennucci, G. A. Petersson, H. Nakatsuji, M. Caricato, X. Li, H. P. Hratchian, A. F. Izmaylov, J. Bloino, G. Zheng, J. L. Sonnenberg, M. Hada, M. Ehara, K. Toyota, R. Fukuda, J. Hasegawa, M. Ishida, T. Nakajima, Y. Honda, O. Kitao, H. Nakai, T. Vreven, J. A. Montgomery, Jr., J. E. Peralta, F. Ogliaro, M. Bearpark, J. J. Heyd, E. Brothers, K. N. Kudin, V. N. Staroverov, T. Keith, R. Kobayashi, J. Normand, K. Raghavachari, A. Rendell, J. C. Burant, S. S. Iyengar, J. Tomasi, M. Cossi, N. Rega, J. M. Millam, M. Klene, J. E. Knox, J. B. Cross, V. Bakken, C. Adamo, J. Jaramillo, R. Gomperts, R. E. Stratmann, O. Yazyev, A. J. Austin, R. Cammi, C. Pomelli, J. W. Ochterski, R. L. Martin, K. Morokuma, V. G. Zakrzewski, G. A. Voth, P. Salvador, J. J. Dannenberg, S. Dapprich, A. D. Daniels, O. Farkas, J. B. Foresman, J. V. Ortiz, J. Cioslowski and D. J. Fox, *Gaussian 09, Revision A.1*, Gaussian Inc., Wallingford CT, 2009.
- 46 H. J. Werner, P. J. Knowles, G. Knizia, F. R. Manby, M. Schütz, P. Celani, W. Györfy, D. Kats, T. Korona, R. Lindh, A. Mitrushenkov, G. Rauhut, K. R. Shamasundar, T. B. Adler, R. D. Amos, A. Bernhardsson, A. Berning, D. L. Cooper, M. J. O. Deegan, A. J. Dobbyn, F. Eckert, E. Goll, C. Hampel, A. Hesselmann, G. Hetzer, T. Hrenar, G. Jansen, C. Köppl, Y. Liu, A. W. Lloyd, R. A. Mata, A. J. May, S. J. McNicholas, W. Meyer, M. E. Mura, A. Nicklaß, D. P. O'Neill, P. Palmieri, D. Peng, K. Pflüger, R. Pitzer, M. Reiher, T. Shiozaki, H. Stoll, A. J. Stone, R. Tarroni, T. Thorsteinsson and M. Wang, *MOLPRO, version 2010.1*, University College Cardiff Consultants Ltd, United Kingdom, 2010, <http://www.molpro.net>.
- 47 Y. Georgievskii, J. A. Miller, M. P. Burke and S. J. Klippenstein, *J. Phys. Chem. A*, 2013, **117**, 12146–12154.
- 48 Y. Georgievskii and S. J. Klippenstein, MESS.2016.3.23, <http://tcg.cse.anl.gov/papr/codes/mess.html>.
- 49 A. M. Mebel, Y. Georgievskii, A. W. Jasper and S. J. Klippenstein, *Faraday Discuss.*, 2017, **195**, 637–670.
- 50 T. Yang, R. I. Kaiser, T. P. Troy, B. Xu, O. Kostko, M. Ahmed, A. M. Mebel, M. V. Zagidullin and V. N. Azyazov, *Angew. Chem., Int. Ed.*, 2017, **56**, 4515–4519.
- 51 Y. Morita, S. Suzuki, K. Sato and T. Takui, *Nat. Chem.*, 2011, **3**, 197–204.
- 52 A. R. Khamatgalimov and V. I. Kovalenko, *Fullerenes, Nanotubes, Carbon Nanostruct.*, 2017, **25**, 128–132.
- 53 A. R. Khamatgalimov, M. Melle-Franco, A. A. Gaynullina and V. I. Kovalenko, *J. Phys. Chem. C*, 2019, **123**, 1954–1959.
- 54 J. Yu, R. Sumathi and W. H. Green, *J. Am. Chem. Soc.*, 2004, **126**, 12685–12700.